Supporting Information

Fluorinated Porous Molecular Crystals: Vapor-Triggered On-Off Switching of Luminescence and Porosity

Hiroshi Sasaki[†], Hiroaki Imoto[†], Takashi Kitao[§], Takashi Uemura[§], Takashi Yumura[‡], Kensuke Naka*[,†]

† Faculty of Molecular Chemistry and Engineering, Graduate School of Science and Technology, Kyoto Institute of Technology, Goshokaido-cho, Matsugasaki, Sakyo-ku, Kyoto 606-8585, Japan.
‡Faculty of Materials Science and Engineering, Graduate School of Science and Technology, Kyoto Institute of Technology, Goshokaido-cho, Matsugasaki, Sakyo-ku, Kyoto 606-8585, Japan.
§ Department of Advanced Materials Science, Graduate School of Frontier Sciences, The University of Tokyo, 5-1-5 Kashiwanoha, Kashiwa, Chiba 277-8561, Japan.

Contents:

1. Materials

Chlorobenzene (PhCl), o-dichlorobenzene (*o*-DCB), m-dichlorobenzene (*m*-DCB), *n*-hexane, cyclohexane, dichloromethane (DCM), chloroform ($CHCl_3$), hexafluorobenaene (HFB), methanol (MeOH), ethyl acetate (AcEt), methyl isobutyl ketone (MIBK) and potassium iodide (KI) were purchased from Nacalai Tesque, Inc. Tetrahydrofuran (THF), diethyl ether (Et_2O), benzene, iodine and *n*-buthyllitium (1.6 M in hexane solution) were purchased from FUJIFILM Wako Pure Chemical Corporation, Ltd. *cis*-Bis(benzonitrile)dichloroplatinum and diisopropylmagunesium chloride lithium chloride complexes (1.3 M in THF solution) were purchased from Sigma-Aldrich Co., Ltd. Other chemicals were purchased from Tokyo Chemical Industry Co., Ltd. All commercially available chemicals were used without further purification. 9-Methyl-9-arsafluorene (**1**) was prepared by following the literature procedure.[1]

2. Measurements

^1H (400 MHz), $^{13}C\{^1H\}$ (100 MHz) ^{19}F-NMR (376 MHz) NMR spectra were recorded on a Bruker DPX-400 spectrometer. The samples were analyzed in $CDCl_3$ using Me_4Si as an internal standard. The following abbreviations are used; s, singlet; d, doublet; t, triplet; q, quartet; m, multiplet. High-resolution mass spectra (HRMS) were obtained on a JEOL JMS-SX102A spectrometer. The UV−vis spectra were recorded on a Jasco spectrophotometer (V-670 KKN). Emission spectra were obtained on an FP-8500 instrument (JASCO), and absolute PL quantum yields (Φ) were determined using a JASCO ILFC-847S instrument; the quantum yield of quinine sulfate reference was 0.52, which is in agreement with the literature value.[2] Differential scanning calorimetry (DSC) was recorded on a DSC-60 Plus (Shimadzu, Kyoto, Japan). Thermogravimetric analysis (TGA) was performed on a DTA-60 (Shimadzu, Kyoto, Japan) under N_2. Powder X-ray diffractometry (XRD) studies were performed on a Rigaku Smartlab X-ray diffractometer with Cu Kα radiation (λ = 1.5406 Å) in the $2\theta/\theta$ mode at room temperature. The 2θ scan data were collected at 0.01° intervals and the scan speed was 10˚ (2θ) / min. The adsorption isotherms of N_2 at 77 K and CO_2 at 195 K were measured by BELSORP-max and BELSORP-mini equipment, respectively. Before the adsorption measurements, the sample was treated under reduced pressure ($<10^{-2}$ Pa) at 373 K for 5 h.

3. X-ray Crystallographic Data for Single-Crystalline Products

The single crystals were mounted on glass capillary. Intensity data were collected at room temperature on a Rigaku XtaLAB mini instrument with graphite-monochromated Mo Kα radiation. Readout was performed in the 0.073 mm pixel mode. The data were collected at room temperature to a maximum 2θ value of 55.0°. Data were processed by Crystal Clear.[3] A numerical absorption

correction[4] was applied. The data were corrected for Lorentz and polarization effects. The structure was solved by direct methods[5] and expanded using Fourier techniques. The non-hydrogen atoms were refined anisotropically. Hydrogen atoms were refined using the riding model. The final cycle of full-matrix least-squares refinement on F^2 was based on observed reflections and variable parameters. All calculations were performed using the CrystalStructure[5] crystallographic software package, except for refinement, which was performed using SHELXL2013.[6] The crystal data has been treated by the PLATON SQUEEZE for the analysis of solvent-containing voids. Crystal data and more information on X-ray data collection are summarized in Tables S1-4.

4. Synthesis

*Synthesis of 9-pentafluorophenyl-9-arsafluorene (**3**)*

A THF (2 ml) solution of iodine (0.456 g, 1.80 mmol) was added into a THF (3 ml) solution of 9-methyl-9-arsafluorene of **1** (0.426 g, 1.76mmol), and the mixture was stirred at 65 °C for 36 h to give 9-iode-9-arsafluorene **2**. Isopropyl magnesium chloride (1.40 ml, 1.82mmol) was added dropwise into a THF (10 ml) solution of bromopentaflurorobenzene (0.439g, 1.78mmol) at -78 °C, the mixture was stirred for 75 min at -78 °C. The prepared nucleophile was added to the THF solution of **2** at 0 °C, the reaction mixture was stirred overnight at room temperature. Distilled water (5ml) was added to the reaction mixture, and extracted with CH_2Cl_2. Collected organic layer was dried with $MgSO_4$, filtrated, and concentrated under reduced pressure. The residue was purified through silica column chromatography (hexane) and recrystallized from CH_2Cl_2 and hexane to obtain **3** as colorless crystals (0.403 g, 58% yield). ^{1}H-NMR ($CDCl_3$, 400 MHz): δ 7.91 (d, 2H, J = 7.6Hz), 7.77 (d, 2H, J = 7.6 Hz), 7.49 (td, 2H, J = 7.6 Hz), 7.33 (td, 2H, J = 7.4 Hz) ppm. ^{13}C{^{1}H}NMR ($CDCl_3$, 100 MHz) δ 149.1-148.8, 146.7-146.5, 146.4, 143.0-142.7, 141.0, 140.5-140.2, 138.7-138.3, 136.1-135.8, 132.1, 129.7, 128.1, 122.2 ppm; ^{19}F-NMR ($CDCl_3$, 376 MHz): δ -128.3, -148.4, -159.1 ppm. HRMS (FAB): calcd for $C_{18}H_8F_5As$ $[M]^+$, 393.9762; found, 393.9756.

*Synthesis of $PtCl_2$(9-pentafluorophenyl-9-arsafluorene)$_2$ (**4**).*

A PhCl (15 ml) solution of **3** (0.1942 g, 0.493 mmol) and cis[$PtCl_2(PhCN)_2$] (0.115 g, 0.245 mmol) was refluxed under N_2 overnight. The solvent was removed in vacuo, and the residue was recrystallized with CH_2Cl_2 and hexane to give **4** as light yellow crystals (0.235 g, 0.223 mmol, 91 %). ^{1}H NMR (CDCl3, 400 MHz): δ 8.26 (d, 4H, J = 7.6 Hz), 7.89 (m, 4H, J = 7.6 Hz), 7.60 (td, 4H, J = 7.6 Hz), 7.43 (td, 6H, J = 7.6 Hz) ppm. ^{19}F-NMR ($CDCl_3$, 376 MHz): δ -125.3, -148.4.1, -159.1 ppm. ^{13}C{^{1}H} NMR were not measured because of the low solubility of the product.

*Synthesis of PtI_2(9-pentafluorophenyl-9-arsafluorene)$_2$ (**5**).*

A PhCl (10 ml) solution of **4** (53.9 mg, 51.1 μmol), MIBK (1 ml), and KI (169.3 mg, 1.02 mmol) was refluxed under N_2 overnight. Distilled water (5 ml) was added to the reaction mixture, which was then extracted with CH_2Cl_2. The solvent was removed in vacuo, and the residue was recrystallized with *o*-dichorobenzene to give porous $\mathbf{5}_{\alpha}$ as red crystals (40.0 mg, 32.3μmol, 63%). The obtained crystals of $\mathbf{5}_{\alpha}$ were subjected to recrystallization from CH_2Cl_2 and hexane, and the crystals of $\mathbf{5}_{\beta}$ were obtained as red crystals quantitatively. ^{1}H NMR ($CDCl_3$, 400 MHz): δ 8.21 (d, 4H, J = 7.6 Hz), 7.88 (d, 4H, J = 7.6 Hz), 7.58 (t, 4H, J = 7.4 Hz), 7.46 (t, 4H, J = 7.4 Hz) ppm. ^{19}F-NMR ($CDCl_3$, 376 MHz) δ -126.4, -150.2, -160.5 ppm.

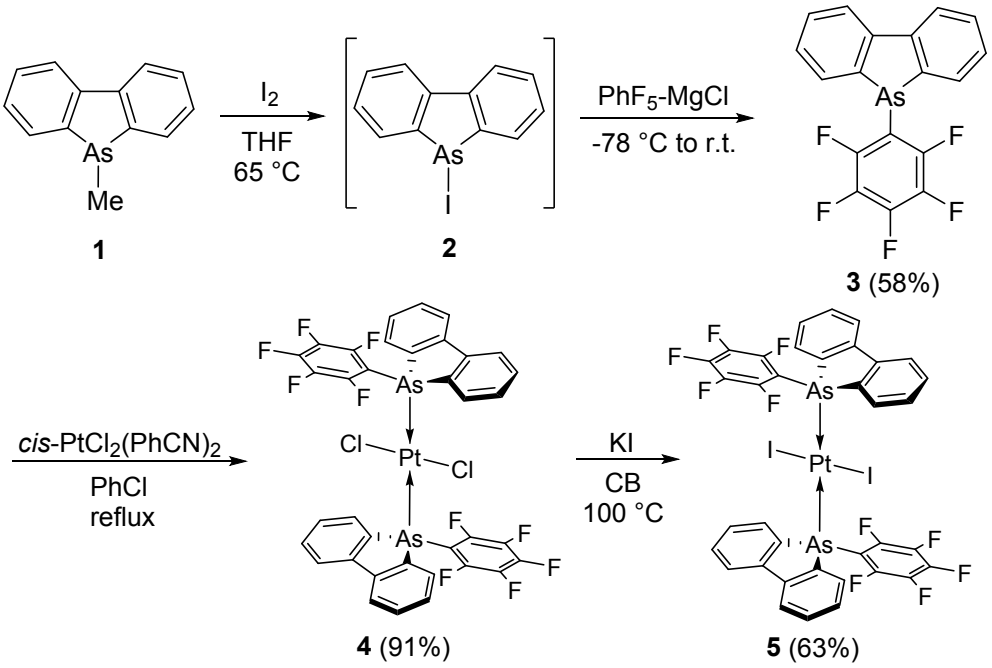

Scheme S1. Synthesis of ligand **3** and platinum(II) complexes **4** and **5**.

5. NMR spectra

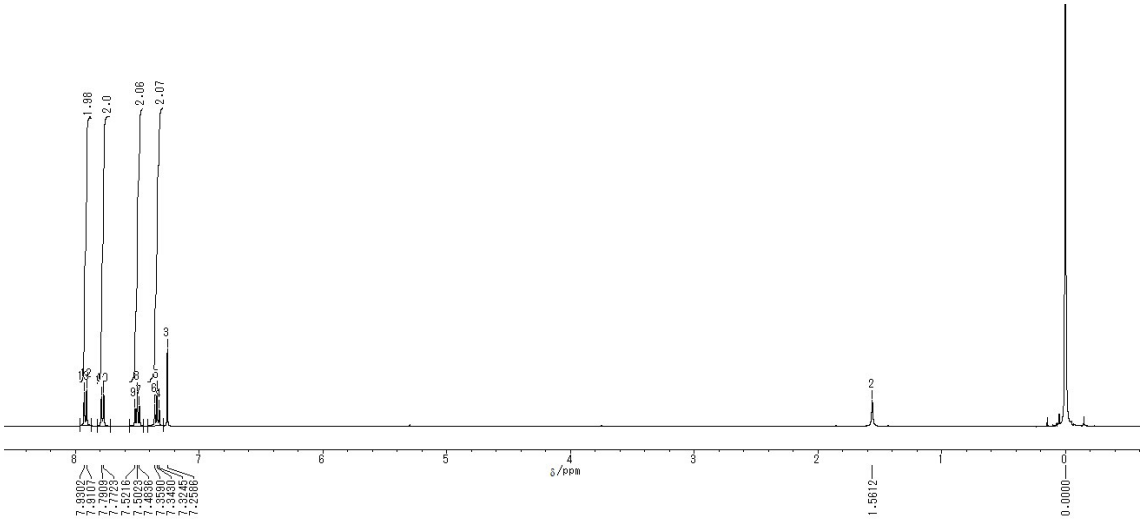

Figure S1. ^{1}H-NMR spectrum (400 MHz) of **3** in $CDCl_3$.

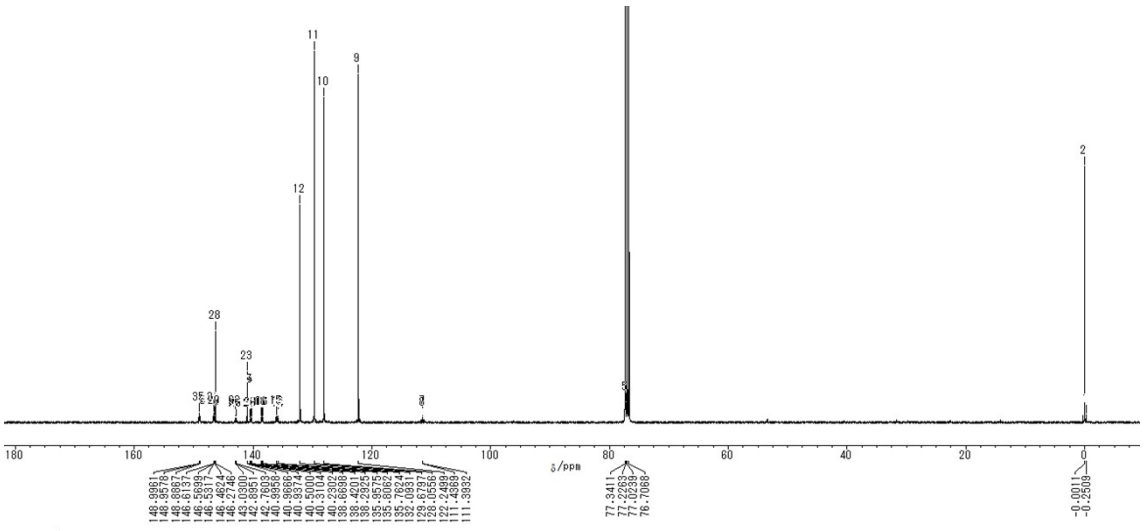

Figure S2. ^{13}C-NMR spectrum (100 MHz) of **3** in $CDCl_3$.

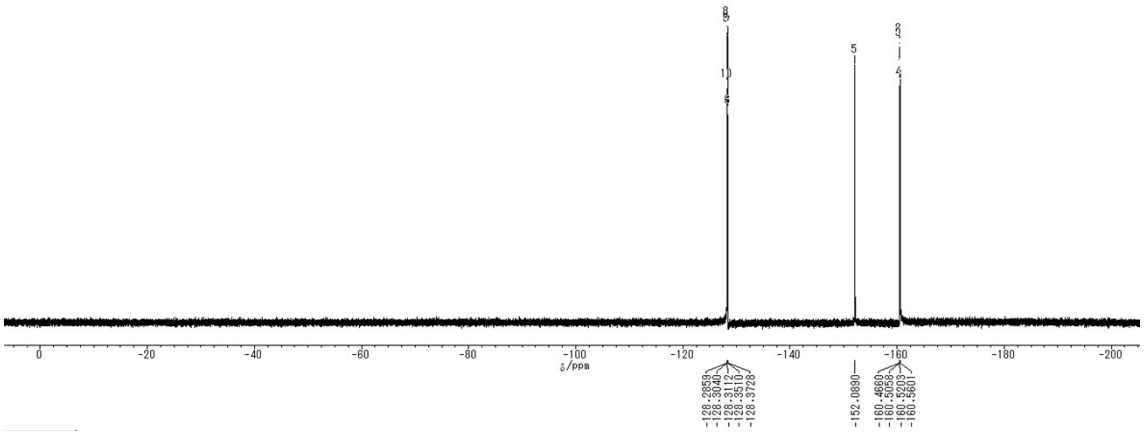

Figure S3. ^{19}F-NMR spectrum (376 MHz) of **3** in $CDCl_3$.

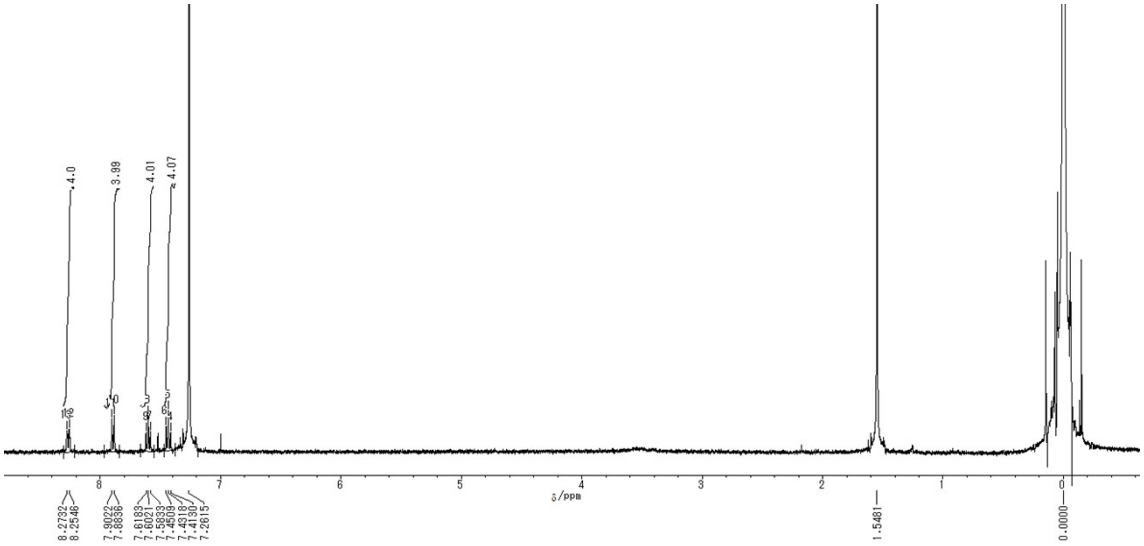

Figure S4. ^{1}H-NMR spectrum (400 MHz) of **4** in $CDCl_3$.

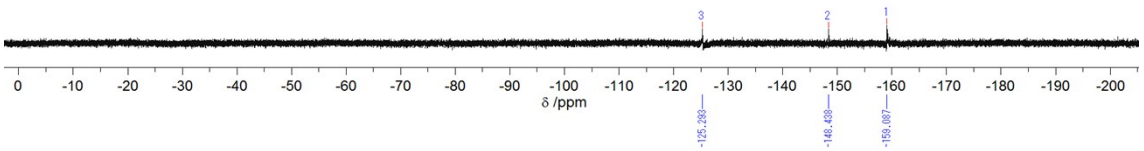

Figure S5. ^{19}F-NMR spectrum (376 MHz) of **4** in $CDCl_3$.

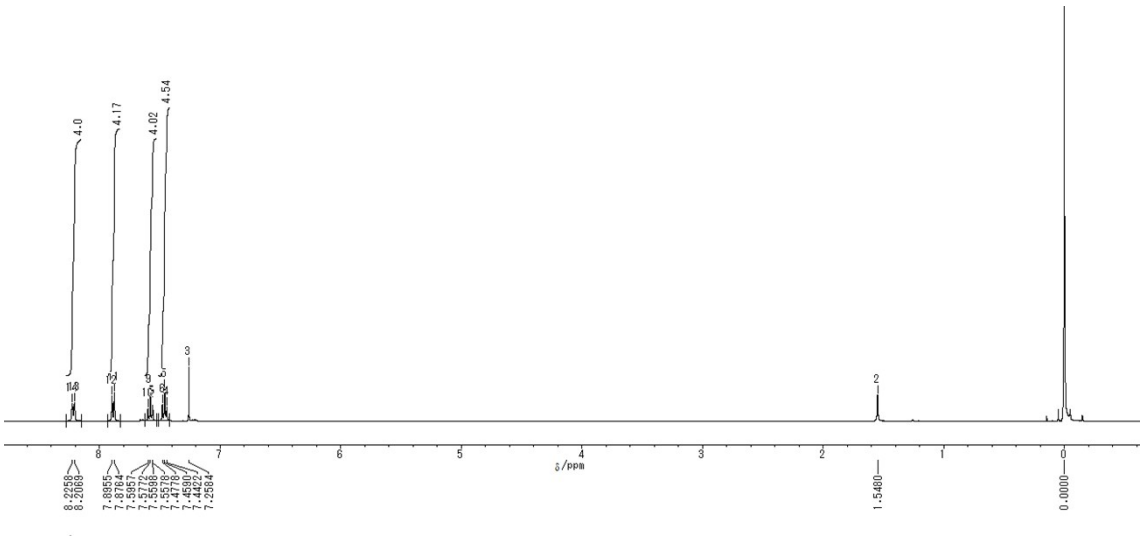

Figure S6. ^{1}H-NMR spectrum (400 MHz) of **5** in CD_2Cl_2.

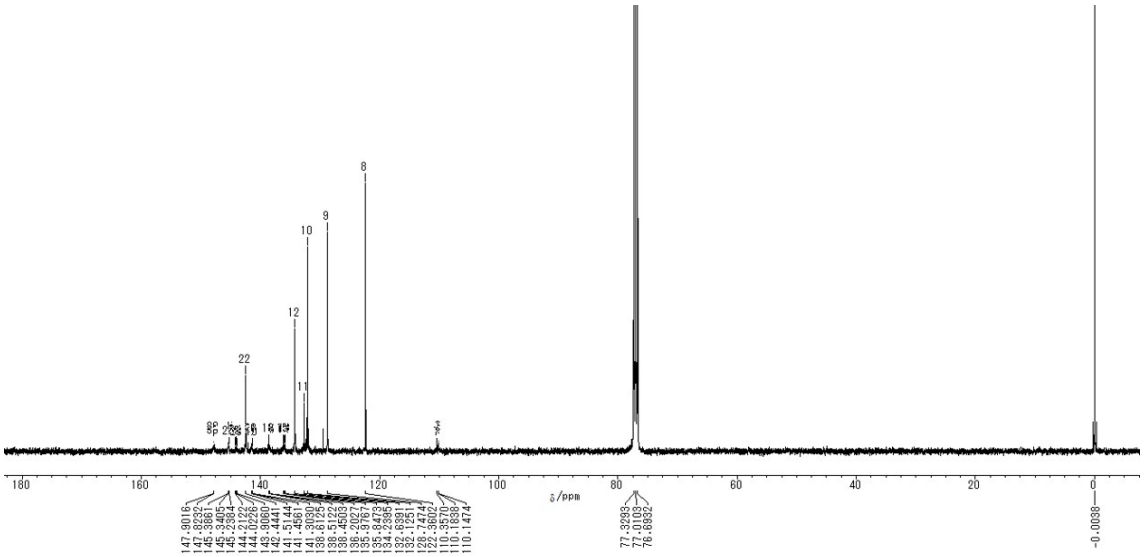

Figure S7. ^{13}C-NMR spectrum (100 MHz) of **5** in $CDCl_3$.

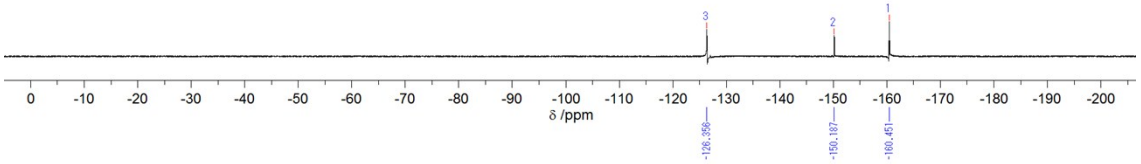

Figure S8. ^{19}F-NMR spectrum (376 MHz) of **5** in $CDCl_3$.

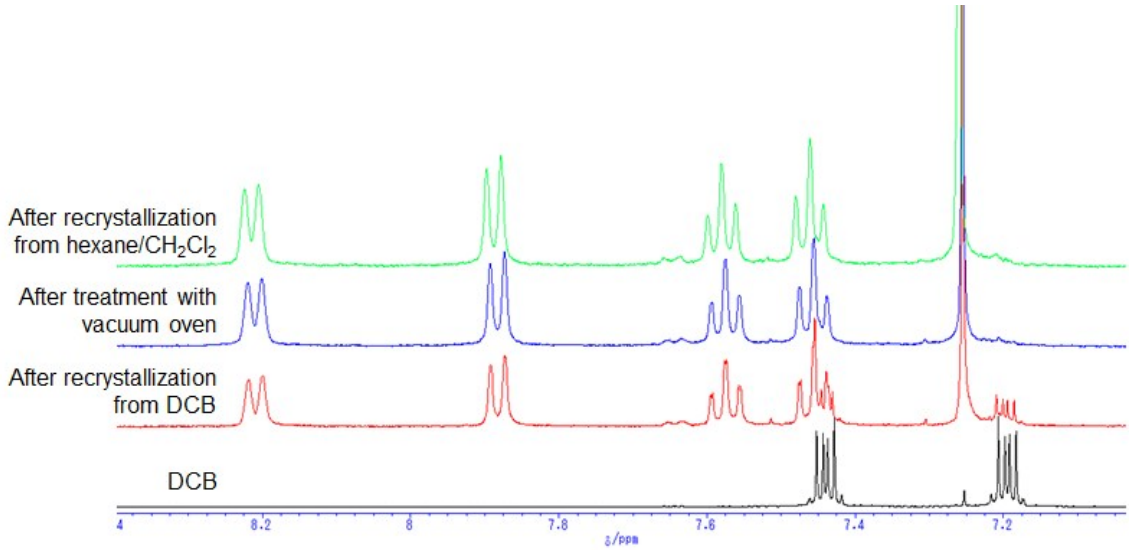

Figure S9. ^{1}H-NMR spectra (400 MHz) in $CDCl_3$: *o*-DCB (black), **5** after recrystallization from *o*-DCB (red), treatment with vacuum oven (blue), and recrystallization from hexane/DCM (green).

6. Crystallographic data

Table S1. Crystallographic Data of **4**, $\mathbf{5}_{\alpha}$, and $\mathbf{5}_{\beta}$.

	4	$\mathbf{5}_{\alpha}$	$\mathbf{5}_{\beta}$
Crystal data			
Empirical Formula	$C_{36}H_{16}As_2F_{10}Cl_2Pt$	$C_{36}H_{16}As_2F_{10}I_2Pt$	$C_{37}H_{18}As_2Cl_2F_{10}I_2Pt$
Formula Weight	1054.35	1237.25	1322.18
Crystal Dimension, mm^3	0.290 × 0.060 × 0.050	0.280 × 0.120 × 0.100	0.390 × 0.230 × 0.150
Crystal System	trigonal	trigonal	triclinic
Space Group	R-3	R-3	P-1
a, Å	33.6076(16)	34.320(3)	15.149(8)
b, Å	33.6076(16)	34.320(3)	16.919(9)
c, Å	8.2710(5)	8.6005(10)	17.071(9)
α, deg	-	-	95.15140(10)
β, deg	-	-	112.313(8)
γ, deg	-	-	104.884(5)
Volume, $Å^3$	8090.3(8)	8772.9(14)	3825(4)
D_{calcd}, g cm^{-3}	1.948	2.108	2.296
Z	9	9	4
F(000)	4500	5148	2456
Data Collection			
Temperature, deg	25.0	25.0	25.0
2θmax, deg	55.0	55.1	55.0
Tmin/Tmax			
Refinement			
No. of Observed Data	4115	4472	17469
No. of Parameters	232	232	946
R1[a], wR2[b]	0.0402, 0.1029	0.0332, 0.0881	0.0658, 0.1845
Goodness of Fit Indictor	1.058	1.027	0.949

[a]$R1 = \Sigma \, | \, |Fo| - |Fc| \, | \, / \, \Sigma \, |Fo|$ [b]$wR2 = [\, \Sigma \, w \, ((Fo^2-Fc^2)^2 \, / \, \Sigma \, w \, (Fo^2)^2 \,]^{1/2}$ $w = [\, \sigma^2(Fo^2) \,]^{-1}$

CCDC #1897958 (**4**), 1897959 ($\mathbf{5}_{\alpha}$), and 1897960 ($\mathbf{5}_{\beta}$).

Table S2. ORTEP drawing (ellipsoids at 50% probability, hydrogen atoms are omitted for clarity), selected distances (Å) and angles (deg) of **4**.

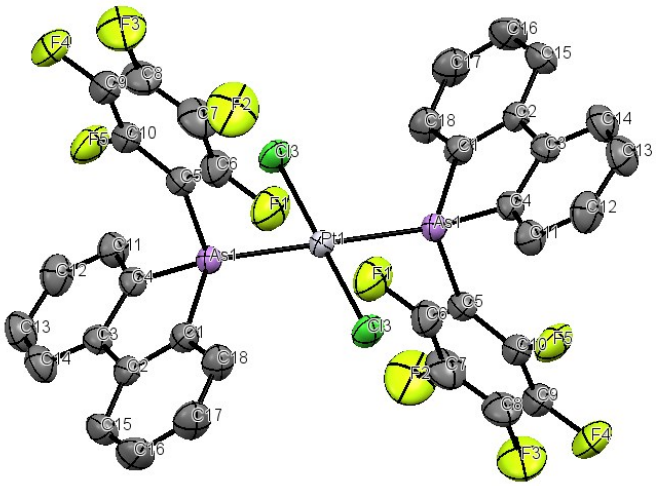

distance(Å)		angles(°)	
Pt(1)-Cl(3)	2.2954(11)	As(1)-Pt(1)-Cl(3)	93.17(5)
Pt(1)-As(1)	2.3853(7)	As(1)-Pt(1)-As(1)	180.00(3)
As(1)-C(1)	1.933(5)	Cl(3)-Pt(1)-Cl(3)	180.00(8)
As(1)-C(4)	1.923(4)	C(1)-As(1)-C(4)	88.63(19)
As(1)-C(5)	1.933(5)	C(1)-As(1)-C(5)	102.9(2)
		C(4)-As(1)-C(5)	106.7(2)

Table S3. ORTEP drawing (ellipsoids at 50% probability, hydrogen atoms are omitted for clarity), selected distances (Å) and angles (deg) of $\mathbf{5}_{\alpha}$.

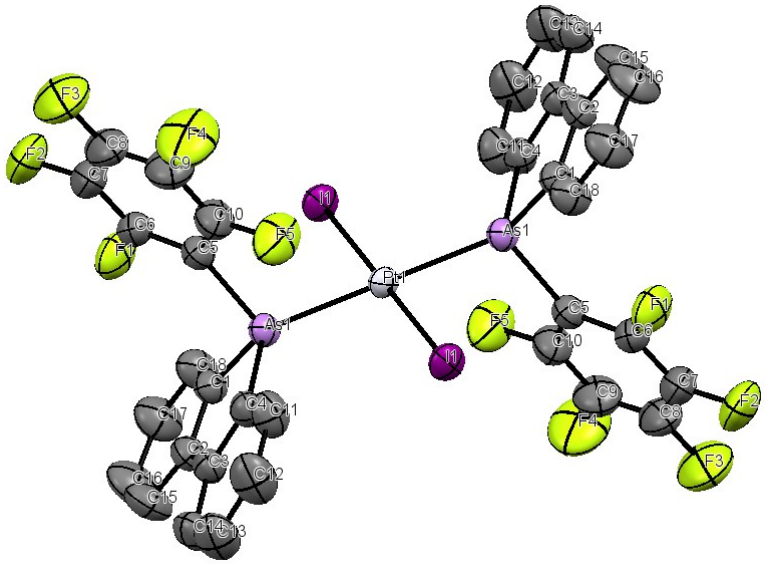

distance(Å)		angles(°)	
Pt(1)-I(1)	2.5812(4)	As(1)-Pt(1)-I(1)	92.695(19)
Pt(1)-As(1)	2.3857(7)	As(1)-Pt(1)-As(1)	180.00(3)
As(1)-C(1)	1.934(4)	I(1)-Pt(1)-I(1)	180.00(3)
As(1)-C(4)	1.939(5)	C(1)-As(1)-C(4)	88.38(18)
As(1)-C(5)	1.953(5)	C(1)-As(1)-C(5)	107.3(2)
		C(4)-As(1)-C(5)	102.3(2)

Table S4. ORTEP drawing (ellipsoids at 50% probability, hydrogen atoms are omitted for clarity), selected distances (Å) and angles (deg) of **5**$_{\beta}$.

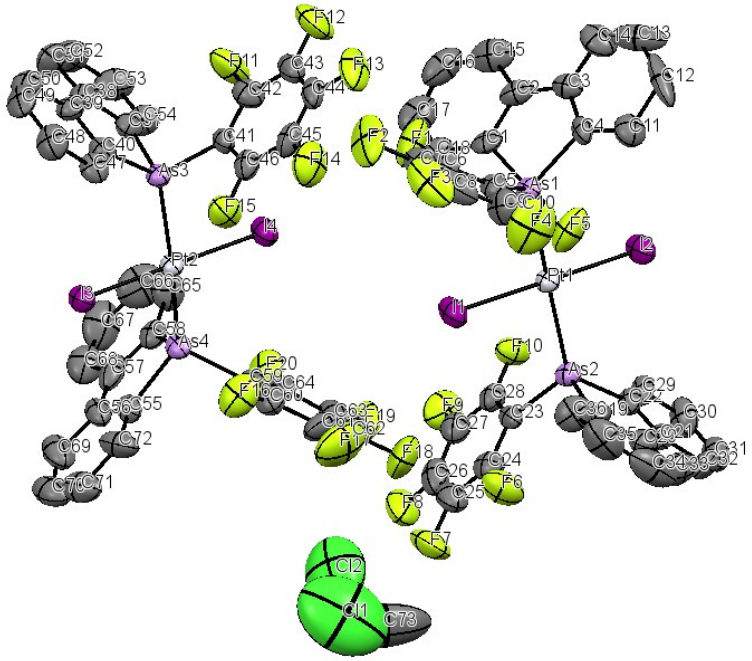

distance(Å)		angles(°)	
Pt(1)-I(1)	2.6112(13)	As(1)-Pt(1)-I(1)	89.49(4)
Pt(1)-I(2)	2.5891(14)	As(1)-Pt(1)-I(2)	90.53(4)
Pt(1)-As(1)	2.3733(18)	As(2)-Pt(1)-I(1)	89.40(4)
Pt(1)-As(2)	2.3779(18)	As(2)-Pt(1)-I(2)	90.68(4)
As(1)-C(1)	1.933(13)	As(1)-Pt(1)-As(2)	175.54(5)
As(1)-C(4)	1.923(11)	I(1)-Pt(1)-I(2)	178.81(4)
As(1)-C(5)	1.941(13)	C(1)-As(1)-C(4)	88.0(5)
As(2)-C(19)	1.898(16)	C(1)-As(1)-C(5)	107.7(5)
As(2)-C(22)	1.935(11)	C(4)-As(1)-C(5)	101.4(5)
As(2)-C(23)	1.938(13)	C(19)-As(2)-C(22)	88.9(5)
Pt(2)-I(3)	2.5913(14)	C(19)-As(2)-C(23)	108.4(6)
Pt(2)-I(4)	2.6140(14)	C(22)-As(2)-C(23)	97.7(5)
Pt(2)-As(3)	2.3748(17)	As(3)-Pt(1)-I(3)	90.45(4)
Pt(2)-As(4)	2.3809(17)	As(3)-Pt(1)-I(4)	89.11(4)
As(3)-C(37)	1.924(14)	As(4)-Pt(1)-I(3)	92.34(4)
As(3)-C(40)	1.948(11)	As(4)-Pt(1)-I(4)	88.51(5)

As(3)-C(41)	1.950(11)	As(3)-Pt(1)-As(4)	167.59(5)
As(4)-C(55)	1.924(13)	I(3)-Pt(1)-I(4)	177.95(4)
As(4)-C(58)	1.913(16)	C(37)-As(3)-C(40)	88.8(5)
As(4)-C(59)	1.939(9)	C(37)-As(3)-C(41)	107.8(5)
		C(40)-As(3)-C(41)	99.9(5)
		C(55)-As(4)-C(58)	87.9(6)
		C(55)-As(4)-C(59)	102.1(5)
		C(58)-As(4)-C(59)	110.1(5)

7. Thermal analyses

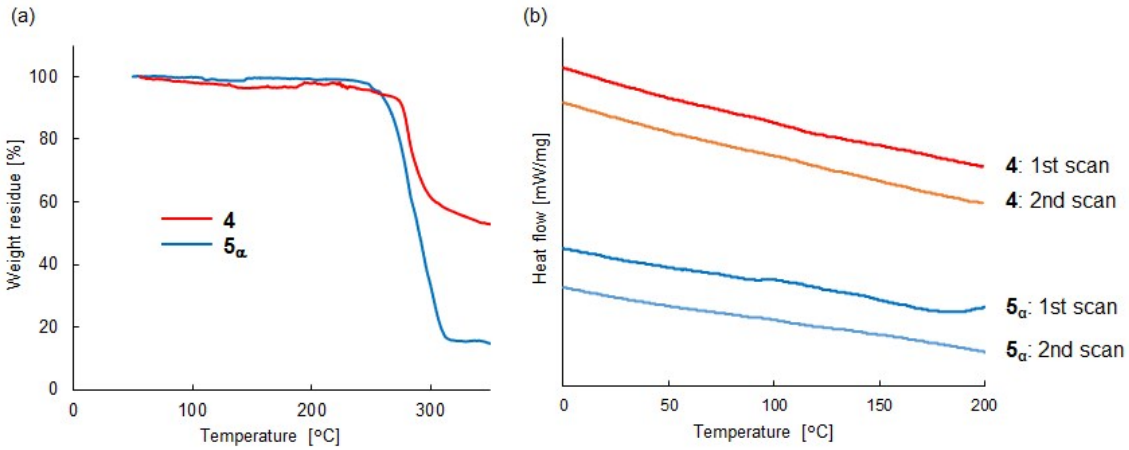

Figure S10. (a) TGA thermograms and (b) DSC traces of **4** and $\mathbf{5_{\alpha}}$.

8. PXRD data

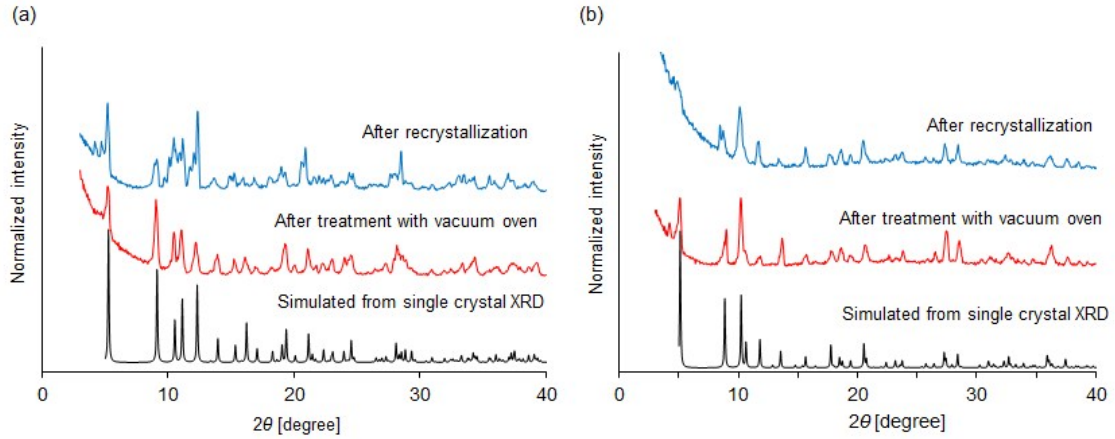

Figure S11. Powder XRD patterns of (a) **4** and (b) $\mathbf{5_{\alpha}}$: after recrystallization (blue) and treatment with vacuum oven (red), and simulated from single crystal XRD (black).

9. Optical properties

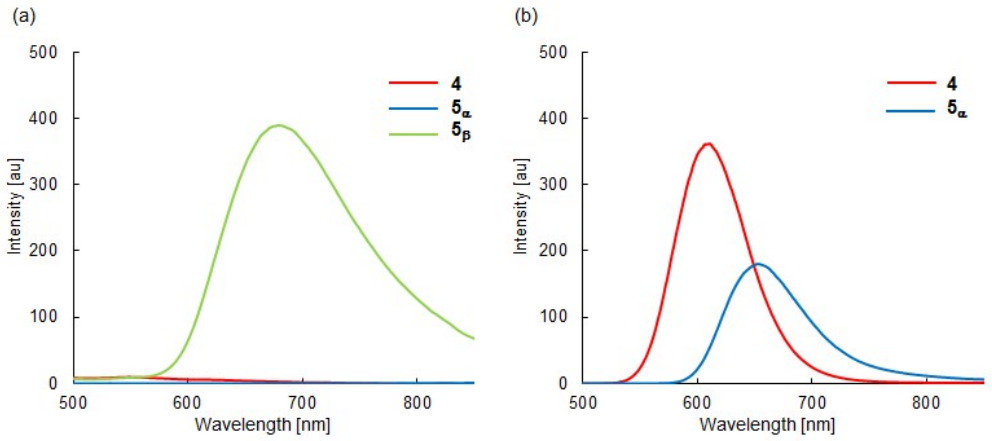

Figure S12. Photoluminescence spectra (excited at 346 nm) of (a) $\mathbf{5_{\alpha}}$ and $\mathbf{5_{\beta}}$ at room temperature, and (b) **4** and $\mathbf{5_{\alpha}}$ at 77 K.

10. Computational study

(A) Stability of PMC structure

Dispersion-corrected DFT calculations (B97D functional) were performed to investigate intermolecular interactions operated between six molecules of **5** in the crystal (Figure S13b) and the full-optimized PMC-hexamer structures (Figure S13a). The 6-31G** basis set was used for C, H, F, and As atoms and the CEP-121G basis set was for Pt and I atoms. The partial- and full optimized PMC-hexamer structures are 20.7 and 18.2 kcal/mol per molecule, and are considered to be stable as compared to the dissociation limit to the six isolated molecules of **5**.

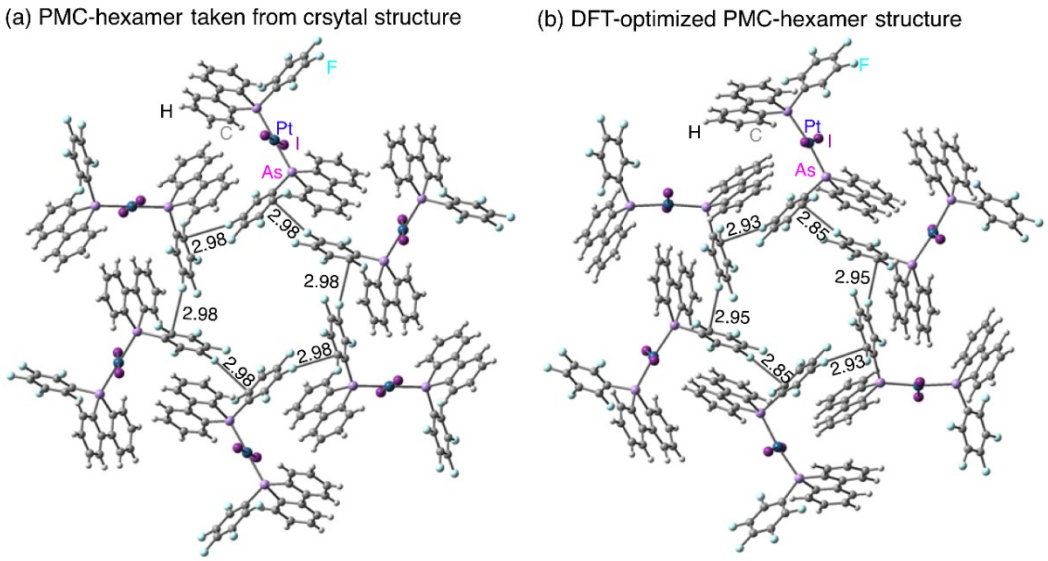

Figure S13. PMC-hexamer structures of $\mathbf{5}_{\alpha}$ (a) taken from the crystal structure as well as (b) obtained from B97D DFT optimization.

The stability can be attributed to at least two types of attractive intermolecular interactions. One is the electrostatic attractive interactions between negatively charged F atoms of the pentafluorophenyl group and positively charged C atoms of the adjacent pentafluorophenyl group of **5**. The electrostatic attractive interactions can be seen confirmed from Figure S14 that displays potential energy surface of approaching of an HFB to the other HFB. In the hexafluorobenzene dimers with a T-shape, one F atom of a HFB points toward six carbon atoms of the other HFB. As shown in Figure S14, the stabilization energy was calculated to be 2.2 kcal/mol in the dimer. The other attractive interactions are due to π-π interactions between an arsafluorene moiety and a positively charged six-membered carbon ring of the pentafluorophenyl group. The attractive π-π interactions can be confirmed by obtaining the ptimized structure for a complex between 9-pentafluorophenyl-9-arsafluorene and HFB

(Figure S15). The optimized structure is stabilized by π-π interactions, whose magnitude was calculated to be 9.3 kcal/mol. The two types of attractive intermolecular interaction are responsible for maintaining the porous structure. In fact, even after the full geometry optimization by using the initial assembly obtained from the crystal structure, a porous structure is preserved because of the attractive intermolecular interactions. For example, the optimized separations between F atoms of the pentafluorophenyl group and C atoms of the adjacent pentafluorophenyl group of **5** are ~2.9 Å, which are similar to those in the crystal structure (~2.98 Å).

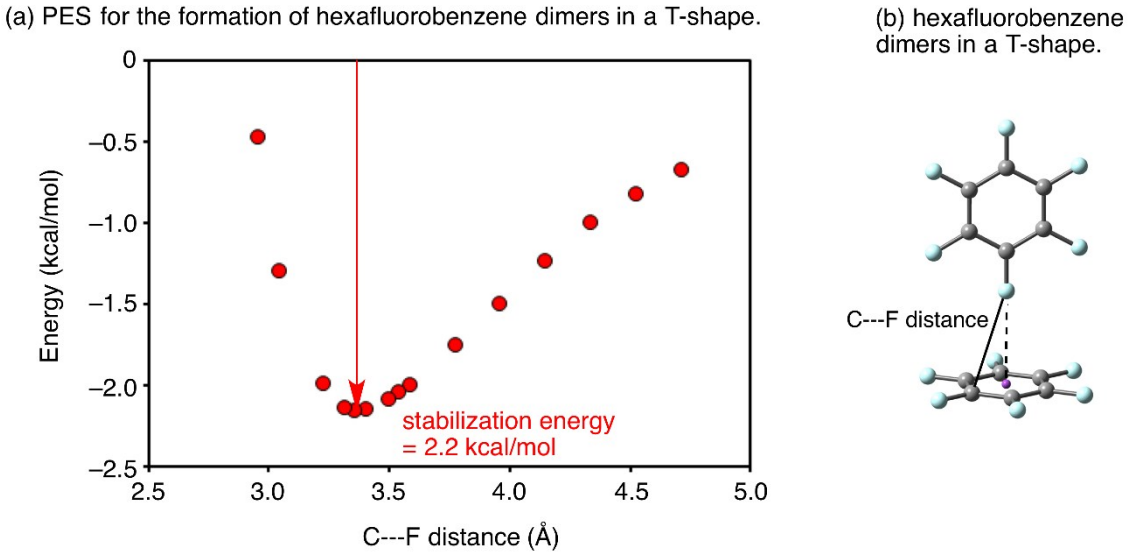

Figure S14. (a) Potential energy surface (PES) of approaching of a hexafluorobenzene into the other hexafluorobenzene to form a hexafluorobenzene dimer with a T-shape (b). The energy of a T-shaped dimer relative to the dissociation limit to two hexafluorobenzene is plotted as a function of the C−F distance defined in (b).

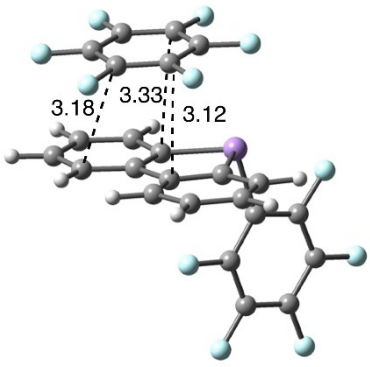

Figure S15. Optimized structure for a complex between 9-pentafluorophenyl-9-arsafluorene and hexafluorobenzene stabilized through π-π interactions.

(B) Interaction between HFB guest and PMC host

Dispersion-corrected DFT calculations were performed to investigate interactions between PMC host and HFB guest. Figure S16 shows structures for HFB inside PMC-hexamer of $\mathbf{5}_{\alpha}$ (HFB@PMC-hexamer) obtained from partial and full optimization. In the partial optimization, atom positions of PMC hexamer were kept to those in the crystal structure. In the optimized structures, some of F atoms are separated by ~3.0 Å from the C atoms of the pentafluorophenyl groups of **5.** The separations indicate the operation attractive electrostatic interactions between negatively charged F atoms and positively charged C atoms, according to potential energy surface in Figure S14a.

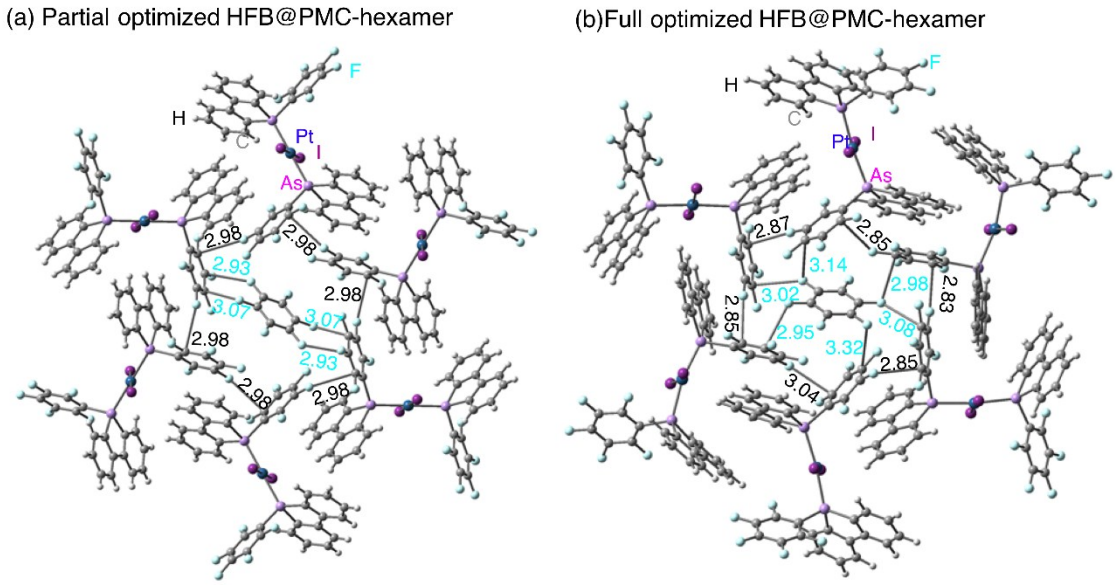

Figure S16. HFB inside PMC-hexamer (HFB@PMC-hexamer) structures of $\mathbf{5}_{\alpha}$ obtained from (a) partial DFT B97D optimization and (b) full optimization. In the partial optimization, atom positions of PMC-hexamer were kept to those in the crystal structure.

(C) Interaction between DCM guest and PMC host or non-PMC

Dispersion-corrected DFT calculations were performed to investigate interactions between DCM guest and PMC or non-PMC host. Figure S17 shows structures for DCM inside PMC-hexamer (DCM@PMC-hexamer) or DCM inside non-PMC-hexamer (DCM@non-PMC-hexamer) obtained from partial optimization. In the partial optimization, atom positions of PMC hexamer were kept to those in the crystal structure.

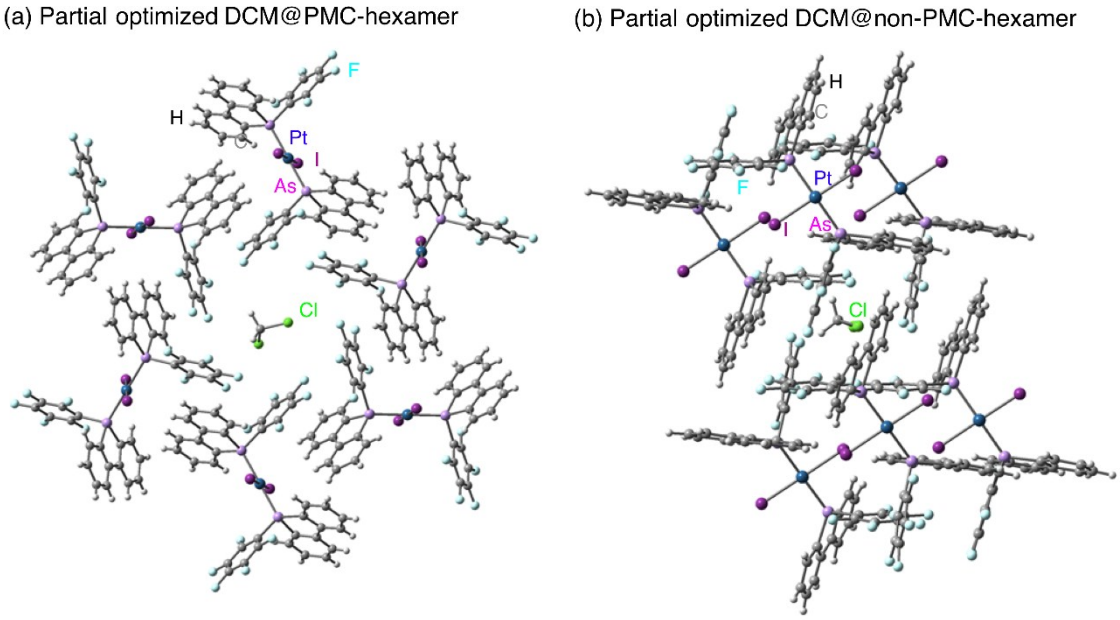

Figure S17. (a) DCM inside PMC-hexamer (DCM@PMC-hexamer) structures and (b) non-PMC-hexamer DCM@non-PMC obtained from partial DFT B97D optimization. In the e partial optimization, atom positions of PMC-hexamer were kept to those in the crystal structure.

(D) Molecular structure of 5 in PMC or non-PMC

We noticed different structures of contained **5** molecules between PMC and non-PMC. We can distinguish the two structures by using the dihedral angle of $C(C_6F_5)$−As---As−$C(C_6F_5)$: the dihedral angle is ~ 0 degree in non-PMC, and that in PMC is ~180 degree. By taking one **5** molecule from PMC and non-PMC crystal, we construct their initial geometries, and optimized them by B97D calculations, as shown in Figure S18(a). The two optimized geometries are almost energetically identical. In addition, we obtained the transition state connecting the optimized geometries, and found the activation energy for the transition between the two optimized geometries was calculated to be 4.0 kcal/mol, as shown in Figure S18(b).

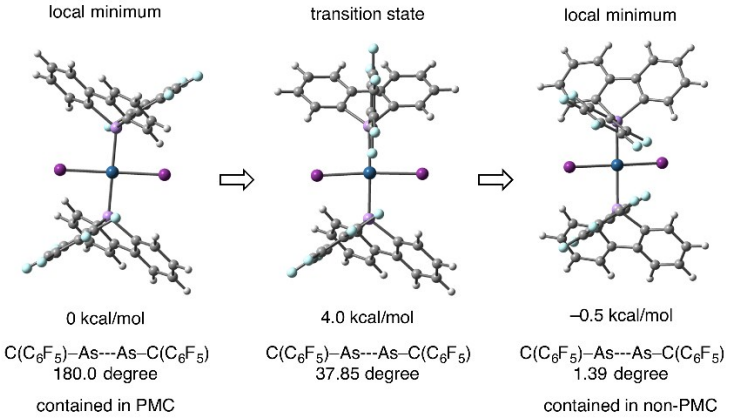

Figure S18. B97D-optimized structures of single molecule **5**, and the transition state connecting the two local minima.

11. Vapochromic luminescence

Table S5. Results of the exposure to various solvent vapor (absolute quantum yield).

Off → On*	Dichloromethane (0.05), ethyl acetate (0.08), benzene (0.02), 1,2-dichloroethane (0.02), diethyl ether (0.07)
No change	Hexane, cyclohexane, perfluorohexane, hexafluoroisopropyl alcohol, methanol, acetonitrile
On → Off	*o*-Dichlorobenzene, *m*-dichlorobenzene, hexafluorobenzene

*THF and Chloroform: soluble

12. Gas adsorption isotherms

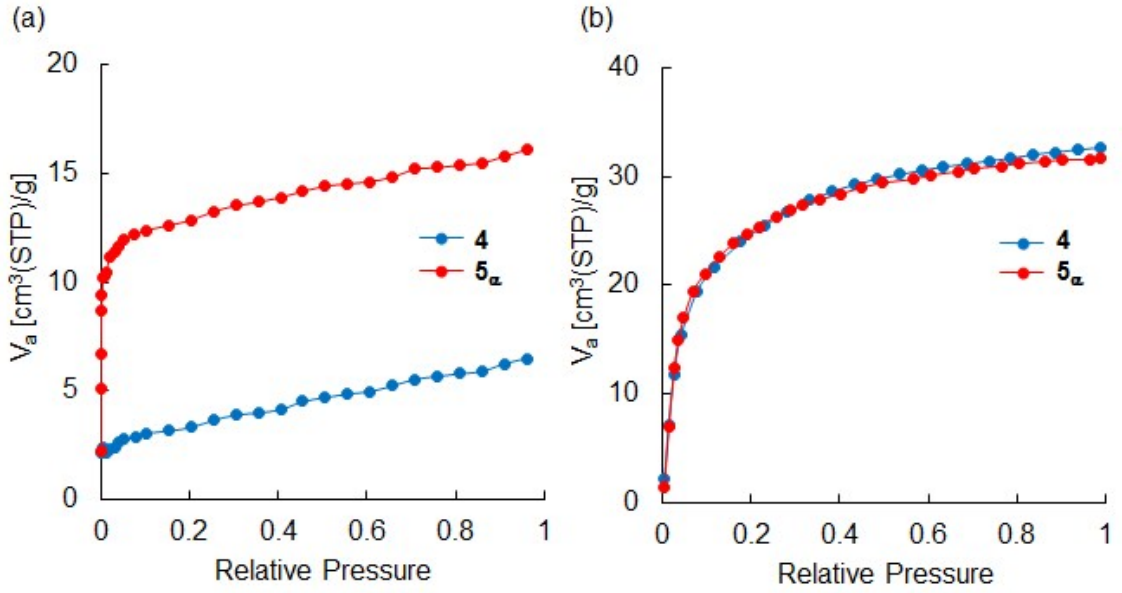

Figure S19. Gas adsorption isotherms of (a) N_2 at 77K and (b) CO_2 at 195 K for **4** and **5**$_\alpha$.

13. References

(1) T. Kato, S. Tanaka, K. Naka, *Chem. Lett.* **2015**, *44*, 1476.

(2) *Fluorescence Measurements, Application to bioscience, Measurement method, Series 3.* Spectroscopical Society of Japan, Academic Publication Center.

(3) *CrystalClear: Data Collection and Processing Software*, Rigaku Corporation (1998-2014). Tokyo 196-8666, Japan.

(4) *SIR2011*: M. C. Burla, R. Caliandro, M. Camalli, B. Carrozzini, G. L. Cascarano, C. Giacovazzo, M. Mallamo, A. Mazzone, G. Polidori, R. Spagna, *J. Appl. Cryst.* **2012**, *45*, 357.

(5) *CrystalStructure 4.1: Crystal Structure Analysis Package*, Rigaku Corporation (2000-2014). Tokyo 196-8666, Japan.

(6) *SHELXL2013*: G. M. Sheldrick, *Acta Cryst.* **2008**, *A64*, 112.